frontiers in Chemistry

ORIGINAL RESEARCH
published: 17 November 2020
doi: 10.3389/fchem.2020.581512

Supported Pt Nanoparticles on Mesoporous Titania for Selective Hydrogenation of Phenylacetylene

*Mingzhen Hu[1,2], Lei Jin[2], Yanliu Dang[3], Steven L. Suib[2,3], Jie He[2,3] and Ben Liu[1]**

[1] Jiangsu Key Laboratory of New Power Batteries, Collaborative Innovation Center of Biomedical Functional Materials, School of Chemistry and Materials Science, Nanjing Normal University, Nanjing, China, [2] Department of Chemistry, University of Connecticut, Mansfield, CT, United States, [3] Institute of Materials Science, University of Connecticut, Mansfield, CT, United States

Semi-hydrogenation of alkynes to alkenes is one of the most important industrial reactions. However, it remains technically challenging to obtain high alkene selectivity especially at a high alkyne conversion because of kinetically favorable over hydrogenation. In this contribution, we show that supported ultrasmall Pt nanoparticles (2.5 nm) on mesoporous TiO_2 (Pt@mTiO_2) remarkably improve catalytic performance toward semi-hydrogenation of phenylacetylene. Pt@mTiO_2 is prepared by co-assembly of Pt and Ti precursors with silica colloidal templates *via* an evaporation-induced self-assembly process, followed by further calcination for thermal decomposition of Pt precursors and crystallization of mTiO_2 simultaneously. As-resultant Pt@mTiO_2 discloses a high hydrogenation activity of phenylacetylene, which is 2.5 times higher than that of commercial Pt/C. More interestingly, styrene selectivity over Pt@mTiO_2 remains 100% in a wide phenylacetylene conversion window (20–75%). The styrene selectivity is >80% even at 100% phenylacetylene conversion while that of the commercial Pt/C is 0%. The remarkable styrene selectivity of the Pt@mTiO_2 is derived from the weakened styrene adsorption strength on the atop Pt sites as observed by diffuse reflectance infrared Fourier transform spectroscopy with CO as a probe molecule (CO-DRIFTS). Our strategy provides a new avenue for promoting alkyne to alkene transformation in the kinetically unfavorable region through novel catalyst preparation.

Keywords: TiO_2, Pt nanocatalysts, mesoporous chemistry, selective hydrogenation, phenylacetylene

OPEN ACCESS

Edited by:
Marc Pera-Titus, Fudan University, China

Reviewed by:
Konstantinos Triantafyllidis, Aristotle University of Thessaloniki, Greece
Mattia Bartoli, Politecnico di Torino, Italy

***Correspondence:**
Ben Liu
ben.liu@njnu.edu.cn

Specialty section:
This article was submitted to Green and Sustainable Chemistry, a section of the journal Frontiers in Chemistry

Received: *09 July 2020*
Accepted: *14 September 2020*
Published: *17 November 2020*

Citation:
Hu M, Jin L, Dang Y, Suib SL, He J and Liu B (2020) Supported Pt Nanoparticles on Mesoporous Titania for Selective Hydrogenation of Phenylacetylene. Front. Chem. 8:581512. doi: 10.3389/fchem.2020.581512

INTRODUCTION

Selective hydrogenation of alkynes to alkenes is one of the most industrially important reactions (Yang et al., 1998, 2019; Mastalir et al., 2000; Huang et al., 2007; Studt et al., 2008; Yuan et al., 2009; Liu H. et al., 2012; Sheng et al., 2012; Tüysüz et al., 2013; Zhao et al., 2015, 2019; Xie et al., 2016; Xiao et al., 2017; Zhan et al., 2017). The increase of alkene selectivity not only benefits high quality of the downstream polyene products but greatly improves the alkene yields and profitability (Borodziński and Bond, 2006, 2008; McCue and Anderson, 2015; Hu et al., 2018a). Pt-based catalysts still suffer from low selectivity to alkenes especially in higher alkyne conversion windows, despite its high activity for hydrogenation (Li et al., 2017; Tang et al., 2017; Wang et al., 2018). In theory, the adsorption and activation of alkynes are favored thermodynamically over Pt compared to alkenes. However, as alkynes approach a high conversion, alkenes become kinetically favorable to adsorb on

Pt, leading to a full hydrogenation to alkanes and thus a sharp decrease in alkene selectivity (Yang et al., 2012; McCue and Anderson, 2015). For example, commercial Pd/C or Pt/C catalysts generally produce alkane at 100% alkyne conversion (Li et al., 2012). The lack of control of alkene selectivity at higher alkyne conversions greatly limits alkene yields. As a result, selective hydrogenation of alkynes is generally conducted at low alkyne conversions to generate enhanced yields of alkenes.

The key to solving this problem lies in developing more efficient Pt-group metal catalysts with weakened alkene adsorption strength, which facilitates the alkenes desorption rather than over hydrogenation to alkanes. Compared with strong σ-bonded alkenes, π-bonded alkenes are more favorable to desorb from the active Pt-group metal (Wan and Zhao, 2007; Armbrüster et al., 2010; Mitsudome et al., 2016; Feng et al., 2017). For example, Li et al. found that the π-bonded ethylene was 0.75 eV more facile than the σ-bonded ethylene to desorb from Pd surfaces based on density-functional theory (DFT) calculations (Feng et al., 2017). This in turn greatly favors high ethylene selectivity where 80% ethylene selectivity is achieved, even when acetylene is fully converted. The π-mode alkene adsorption is mainly on atop metal sites (Pei et al., 2017). To improve the alkene selectivity in selective hydrogenation of alkyne, both nanoparticles (NPs) downsizing and alloying strategies have been carried out to enrich the atop sites of Pt-group metal catalysts (Hu et al., 2018b). On the other hand, metal-support interaction has long been employed to tune catalytic properties of catalysts especially the small NPs with strong interactions with supports (Teschner et al., 2008). A reduced hydrogen reduction temperature is generally observed on the small NPs functionalized supports, which greatly benefits hydrogenation activity by virtue of strong hydrogen spillover (Wang et al., 2015; Wei et al., 2018). The decrease of particle sizes also enables more surface-exposed and low-coordinated active sites in the form of corner or edge sites, potentially favoring weak π-adsorbed alkenes (Kleis et al., 2011; Yang et al., 2013; Wu et al., 2019). Thus, smaller Pt NPs hold great potential to catalyze semi-hydrogenation of alkynes with high catalytic activity and alkene selectivity.

In the current study, we present a highly selective catalyst that contains ultrasmall Pt NPs (2.5 nm), strong Pt-support (Pt-TiO$_2$) interaction, and high surface area (mesoporous framework) for selective hydrogenation of phenylacetylene to styrene. Supporting ultrasmall Pt NPs on mesoporous TiO$_2$ (Pt@mTiO$_2$) were prepared using an evaporation-induced self-assembly (EISA) method (**Figure 1a**). For this synthesis, platinum acetylacetonate (Pt(acac)$_2$) was mixed with titanium sources and structure-directing polymers in EISA (Liu X. et al., 2012). Upon annealing, ultrasmall Pt NPs were synthesized and encapsulated within the ordered mTiO$_2$ support. The ordered mesopores of mTiO$_2$ provide a powerful nanoconfinement and endow the ultrasmall Pt nanoparticles with excellent size uniformity and thermal stability. The monodisperse Pt NPs with sizes of around 2.5 nm remained stable after calcination at 450°C. Pt NPs supported on mTiO$_2$ (Pt@TiO$_2$) exhibited excellent catalytic properties toward selective hydrogenation of phenylacetylene. The selectivity to styrene remained at 100% in the phenylacetylene conversion range of 20–75%. Even at 100% phenylacetylene conversion, Pt@TiO$_2$ exhibited >80% styrene selectivity. The abundant surface atop Pt sites of the Pt@mTiO$_2$ accounted for the high styrene selectivity as revealed by CO-DRIFTS. In addition, the specific mass activity of the 2.5 nm Pt@mTiO$_2$ reached as high as 0.5 mol h^{-1} per gram of Pt metal, which is 2.5 times higher than that of the commercial Pt/C catalyst (0.2 mol h^{-1} per gram of Pt metal).

EXPERIMENTAL SECTION

Chemicals and Materials

Titanium chloride (TiCl$_4$), titanium tetraisopropoxide (TIPO), 1,4-dioxane, phenylacetylene, commercial Pt/C (5 wt%) and platinum acetylacetonate (Pt(acac)$_2$) were purchased from Sigma-Aldrich. The CDCl$_3$ was purchased from Cambridge Isotope Laboratories, Inc. All the chemicals were used without further purification unless otherwise noted. Silane-containing block copolymers of poly(ethylene oxide)-*block*-poly(3-(trimethoxysilyl)propyl methacrylate) (PEO-*b*-PTMSPMA, $M_n = 56.9$ kg mol^{-1}) was prepared through atom transfer radical polymerization (ATPR) method as described in our previous reports (Tauster et al., 1978; Wang et al., 2015; Zhang et al., 2015; Feng et al., 2017; Hu et al., 2020). The polymer micelles were prepared in water/ethanol mixtures and dialyzed in ethanol prior to use. Deionized water (High-Q, Inc. 103S Stills) with a resistivity of >10.0 MΩ was used in all experiments.

Synthesis of Pt@mTiO$_2$

Pt@mTiO$_2$ was prepared using an EISA method. In a typical synthesis, 400 μL of newly prepared TiCl$_4$ solution (10 % in ethanol, volume ratio) was added to 5.0 mL of PEO-*b*-PTMSPMA micelles solution (15.0 mg mL^{-1} in ethanol) under stirring. Two hundred and seventy micro liter of TIPO was then added into the above solution, followed by mild stirring for 30 min. 2.0 mg of Pt(acac)$_2$ dissolved in 1.0 mL of ethanol was added dropwise where the theoretical mole ratio of Pt to Ti is 0.004 (corresponding to 1.0 wt% Pt loading in the obtained Pt@mTiO$_2$). After sufficient stirring for 30 min, the mixture solution was transferred into a Petri dish to evaporate the solvent at 40°C for 24 h and 100°C for another 12 h. After this procedure, the obtained intermediates were allowed for calcination at 450°C under air for 2 h. A template removal process is further carried out by washing with hot 2.0 M NaOH solution for 30 min at 50°C. The Pt loading given by EDS measurements is 1 wt%, agreeing well with the initial Pt feed ratio. Through subsequent drying in vacuum at 50°C overnight, Pt@mTiO$_2$ was finally obtained. About 3.6 nm Pt NPs on mesoporous TiO$_2$ is also prepared as a control using similar procedures except that the thermal calcination is carried out at 650°C for 2 h.

Selective Hydrogenation of Phenylacetylene Catalytic Evaluations

Selective hydrogenation of phenylacetylene over the Pt@mTiO$_2$ catalysts was carried out by the following procedures. Firstly, 10.0 mg of catalyst was added to 3.0 mL of 1,4-dioxane in a 15 mL processed glass bottle. After 20 min sonication, 100.0 mg (1.0

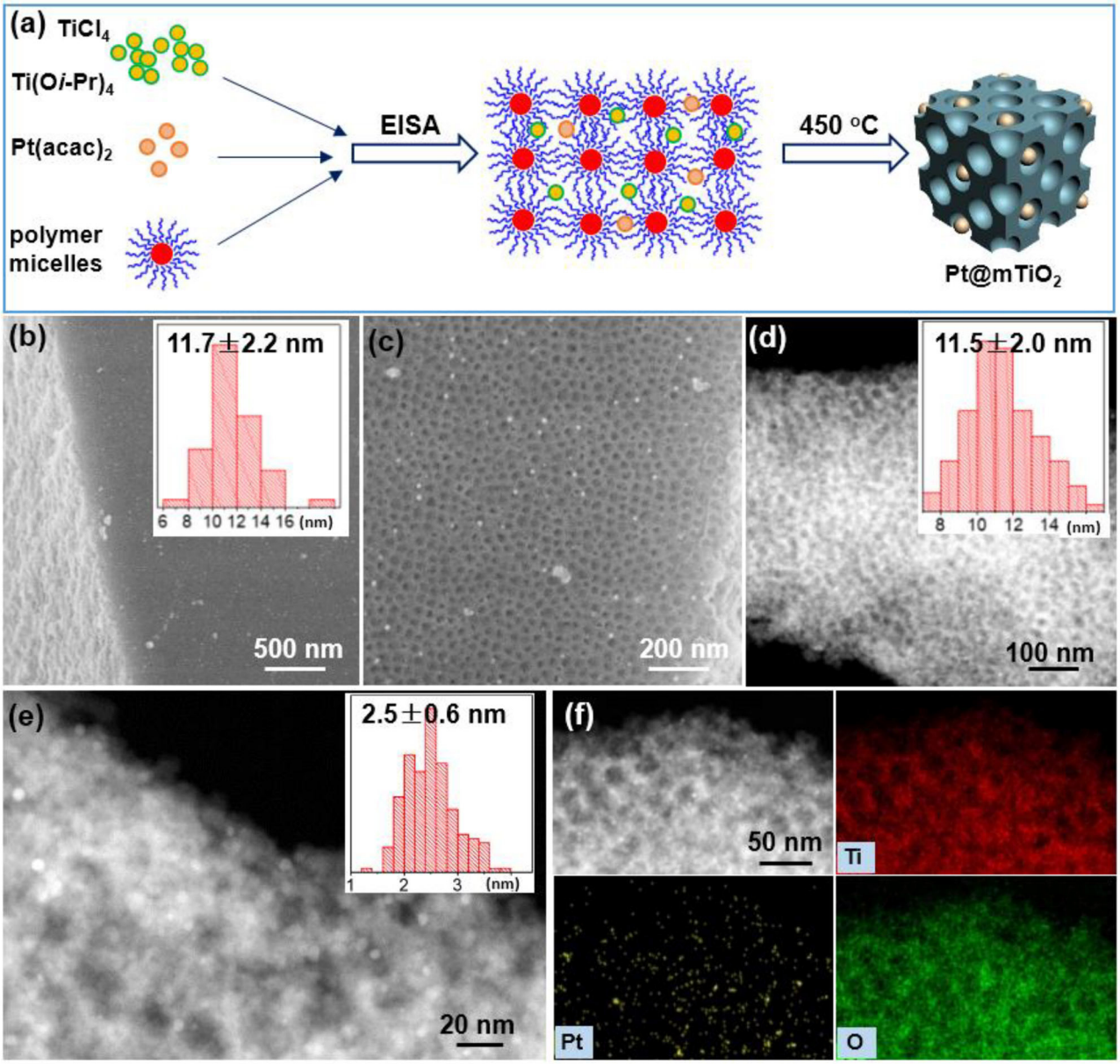

FIGURE 1 | (a) Schematic illustration of preparing 2.5 nm Pt NPs supported within the mesoporous TiO_2. **(b,c)** SEM images, **(d,e)** HAADF-STEM images, and **(f)** EDS mapping images of Pt@mTiO_2. The inset of **(b,d,e)** are size/diameter distributions of mesopores from SEM, mesopores from TEM, and Pt NPs from STEM.

mmol) of phenylacetylene was further added to the homogeneous suspension and stirred for another 30 min. Before transferring the processed bottle to a 25 mL high-pressure stainless-steel reactor, the magnet is taken out, leaving the reaction happen at static conditions without stirring. After purging with hydrogen several times, the reactor was pressurized with 50 psi (pounds per square inch) hydrogen and reacted for varied times. After the reaction finished, the whole reactor was cooled down in an ice bath. The postreaction suspension was separated by centrifugation at 8,000 rpm. The resultant product was kept in a 5 mL test tube and the proton nuclear magnetic resonance (^{1}H NMR) analysis was carried out using $CDCl_3$ as solvent to calculate the conversion of phenylacetylene and the selectivity to styrene. The reaction kinetics were measured both for the Pt@mTiO_2 and commercial Pt/C catalysts. The specific reaction rate was determined as the consumption rate of the phenylacetylene (normalized to the mass of Pt metal per hour) by controlling the phenylacetylene conversion in the kinetic region. The specific rate in this work was calculated using the following equation:

$$r = \frac{N}{w*t} \tag{1}$$

where r is the specific rate, N is the converted phenylacetylene amount in mole, w is supported metal loading weight (gram), and t is the reaction (minute).

The turnover frequency (TOF) is calculated based on the following equation:

$$TOF = \frac{N}{(w/M)*D*t} \quad (2)$$

where N is the converted phenylacetylene amount in mole, w is supported Pt loading weight (gram), M is the molar mass of Pt, D is metal dispersion of Pt and t is the reaction (second). The metal dispersion is calculated according to previous reports (Dominguez-Dominguez et al., 2008; Qiao et al., 2011).

The stability tests of the Pt@mTiO$_2$ and the commercial Pt/C were carried out by recycling the catalyst for 5 consecutive cycles.

Characterization

Scanning electron microscopy (SEM) was conducted on a FEI Nova NanoSEM 450. Bright and dark-field transmission electron microscopy (TEM) was performed on JEM-2100F FETEM. The X-ray diffraction (XRD) patterns were collected on a Bruker D2 Phaser. The small angle X-ray scattering (SAXS) patterns were recorded on a Bruker Nano STAR instrument. X-ray photoelectron spectroscopy (XPS) analysis was conducted on ESCALAB 250 Xi X-ray photoelectron spectrometer with Al Kα radiation. The N_2 sorption measurements were conducted on a Micromeritics ASAP 2020 Surface Area and Porosity Analyzer. ^{1}H NMR spectroscopy was collected on a Bruker Avance 300 MHz spectrometer. Diffuse reflectance Fourier transform infrared (DRIFT) spectroscopy was carried out using a Nicolet IS50 spectrometer using CO as a probe molecule. The DRIFT cell was filled with 20 mg of catalysts and was treated at 100°C with nitrogen before CO was introduced.

RESULTS AND DISCUSSION

Mesoscopic and microscopic structures of the Pt@mTiO$_2$ were thoroughly characterized with SEM and high-angle annular dark field scanning TEM (HAADF-STEM) (**Figure 1**). The SEM image in **Figure 1b** shows the mesopores throughout entire mTiO$_2$ support. **Supplementary Figure 1** shows that mTiO$_2$ displays bulk cubic morphology with a broad side length distribution. The zoomed-in SEM picture in **Figure 1c** confirms the uniform distribution of mesopores. The average pore size of mTiO$_2$ is 11.7 ± 2.2 nm as given in the inset of **Figure 1b**. Since Pt NPs are small, there is no obvious contrast on bright field TEM. The HAADF-STEM technique is further used to identify the ultrasmall Pt NPs. The HAADF-STEM images of Pt@mTiO$_2$ in **Figures 1d–f** reveal the well-dispersed Pt NPs. Pt NPs with a higher electron density are brighter under dark-field STEM image while TiO$_2$ is darker. The average size of Pt NPs is 2.5 ± 0.5 nm as plotted in **Figure 1e**. The pore size of mTiO$_2$ is about 11 nm from HAADF-STEM characterization, which agrees well with the above SEM observations. **Figure 1f** shows energy dispersive X-ray spectroscopy (EDS) mapping images of Pt@mTiO$_2$, further confirming fine dispersion of these 2.5 nm Pt NPs in mTiO$_2$ support. The Pt loading of Pt@mTiO$_2$ is further determined by EDS measurements. As show in **Supplementary Figure 2** and **Supplementary Table 1**, the Pt loadings obtained by EDS measurements of Pt@mTiO$_2$ are about 1 wt%, agreeing well with the initial feed ratio (1 wt%). This observation implies no loss of Pt during preparation processes. By comparison, we have also carried out TEM observations of the commercial Pt/C catalyst. As displayed in **Supplementary Figure 3**, the Pt NPs in commercial Pt/C show a very wide size distribution averaging about 3 nm as reported previously (Cui et al., 2019). The Pt loading of the commercial Pt/C is 5 wt% as received.

To examine the mesoporous structures and crystallographic information of the Pt@mTiO$_2$, we carried out small-angle X-ray scattering (SAXS) and wide-angle X-ray diffraction (XRD) characterization. **Figure 2A** is the SAXS patterns of the Pt@mTiO$_2$ and the pure mTiO$_2$ support. These data show a set of strong scattering peaks that are clearly identified and assigned to (111), (311), and (500) reflections of the face-centered cubic (fcc) mesostructure. The average cell parameters were calculated to be 38 nm as displayed in **Supplementary Table 2**. The SAXS signals are almost the same for Pt@mTiO$_2$ and mTiO$_2$, indicating well-defined mesoporous structures. **Figure 2B** displayed the wide-angle XRD patterns, suggesting the anatase TiO$_2$ phase for both Pt@mTiO$_2$ and mTiO$_2$ (JCPDS 00-064-0863). Unfortunately, due to the ultrasmall size, metallic Pt NPs (JCPDS 04-0802) only showed very broad and weak XRD diffraction (Xiang et al., 2011; Prinz et al., 2014). Benefiting from the well-defined mesoporous structures, the BET specific surface area of the Pt@TiO$_2$ is 42 m^2g^{-1} with an average of pore size of 14 nm as displayed in **Figures 2C,D**.

Pt@mTiO$_2$ has multiple advantageous properties, including ultrasmall Pt NPs and mesoporous framework with high surface area, which possibly benefit the selective hydrogenation of alkynes to alkenes. In this manuscript, selective hydrogenation of phenylacetylene was chosen as a probe reaction since the semi-hydrogenation product of styrene is industrially important (**Figure 3A**). As a control, commercial Pt/C was also investigated. Pt@mTiO$_2$ was favorable for catalyzing the hydrogenation of phenylacetylene to styrene, while commercial Pt/C fully hydrogenated phenylacetylene to ethylbenzene. **Figure 3B** showed the phenylacetylene conversion and the styrene selectivity over Pt@mTiO$_2$ as a function of reaction time. Phenylacetylene was selectively converted to styrene in a wide phenylacetylene conversion window (20–75%), only when phenylacetylene reached full conversion, styrene selectivity slightly dropped to 80.3%. This result (80.3% styrene selectivity at 100% phenylacetylene conversion) is among the best reported to date as demonstrated in **Supplementary Table 3** (Zhao et al., 1998; Kleis et al., 2011; Behrens et al., 2012; Montesano Lopez, 2014; Alig et al., 2019; Han et al., 2019). By comparison, pure mTiO$_2$ is inactive and shows no activity to convert phenylacetylene in the reaction time range from 7 to 26 h (**Supplementary Figure 4**). We have also compared the catalytic properties of Pt@mTiO$_2$ with commercial Pt/C catalysts. Phenylacetylene was fully over hydrogenated to ethylbenzene in the measuring time range from

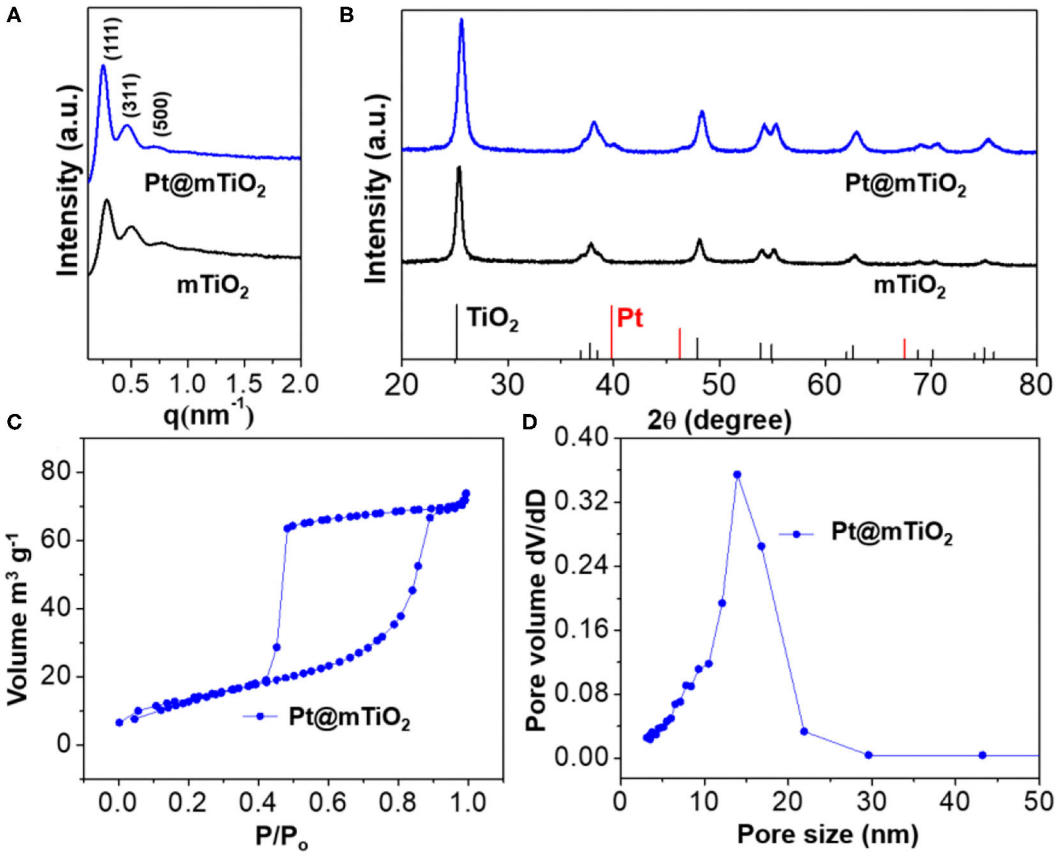

FIGURE 2 | (A) SAXS, and **(B)** wide-angle XRD of Pt@mTiO$_2$ and pure mTiO$_2$. **(C)** N$_2$ adsorption-desorption isotherms, and **(D)** pore size distributions of Pt@mTiO$_2$.

7 to 26 h with a 100% ethylbenzene selectivity as shown in **Supplementary Figure 5**.

Figure 3C shows the catalytic rates of Pt@mTiO$_2$ and commercial Pt/C normalized to the Pt mass per unit time. By controlling the phenylacetylene conversion in the kinetic region (10–20% of conversion), the rate characterizes the intrinsic activity of the catalyst. The catalytic rate of Pt@mTiO$_2$ is 0.5 mol g_{Pt}^{-1} h^{-1}, 2.5 times higher than that of commercial Pt/C (0.2 mol g_{Pt}^{-1} h^{-1}). In addition, the TOF value of the Pt@mTiO$_2$ is calculated to be 4.1 s^{-1}, which is more than 2 times that of the commercial Pt/C (2.0 s^{-1}), demonstrating a higher intrinsic activity. According to previous results, the particle size of Pt NPs is intimately connected with the amount of surface-exposed active sites, which in turn affects the activity (Zhang et al., 2007; Qiao et al., 2011). The smaller sized Pt in Pt@mTiO$_2$ results in more exposed surface Pt sites compared with commercial Pt/C (average size of 3 nm), which benefits high catalytic activity. Catalytic stability is another concern for practical applications. To test the catalytic stability of Pt@mTiO$_2$, we have carried out recycling experiments of the post-reacted Pt@mTiO$_2$ at 50°C and 50 psi hydrogen. As shown in **Figure 3D**, styrene selectivity remains around 80% over the Pt@mTiO$_2$ while phenylacetylene conversion remains at 100% even after five catalytic recycles, showing excellent catalytic stability. By comparison, styrene selectivity over the commercial Pt/C is 0% for the five consecutive measurements at 100% phenylacetylene conversion as displayed in **Supplementary Figure 6**. By virtue of the nanoconfinment enabled by mesoporous mTiO$_2$ supports, the average particle size of the post-reacted Pt@mTiO$_2$ remains the same without any growth or aggregation as displayed in **Supplementary Figure 7**.

To reveal the intrinsic nature why Pt@mTiO$_2$ presented excellent catalytic properties for the selective hydrogenation of phenylacetylene, the surface properties of Pt were carefully studied. We first carried out X-ray photoelectron spectroscopy (XPS) for Pt@mTiO$_2$. **Figure 4A** is the high-resolution Pt 4f XPS spectra of Pt@mTiO$_2$ and commercial Pt/C. The well-resolved XPS binding energy peaks centered at 71.9 and 75.3 eV of Pt@mTiO$_2$ are ascribed to metallic Pt $4f_{7/2}$ and Pt $4f_{5/2}$, respectively. For the commercial Pt/C, the Pt $4f_{7/2}$ and Pt $4f_{5/2}$ shifted to a slightly higher binding energy at 72 and 75.4 eV, respectively. The shift of Pt 4f peaks is indicative of the surface electron density difference of the two samples. 2.5 nm Pt NPs is slightly electron-rich compared to that of the commercial Pt/C. The electron-rich 2.5 nm Pt NPs are more effective to transfer electrons to the π^* molecular orbitals of phenylacetylene, which in turn promotes phenylacetylene activation and improves catalytic reactivity (Wan and Zhao, 2007). Both the Pt@mTiO$_2$ and commercial Pt/C show existence of Pt^{2+} species as identified

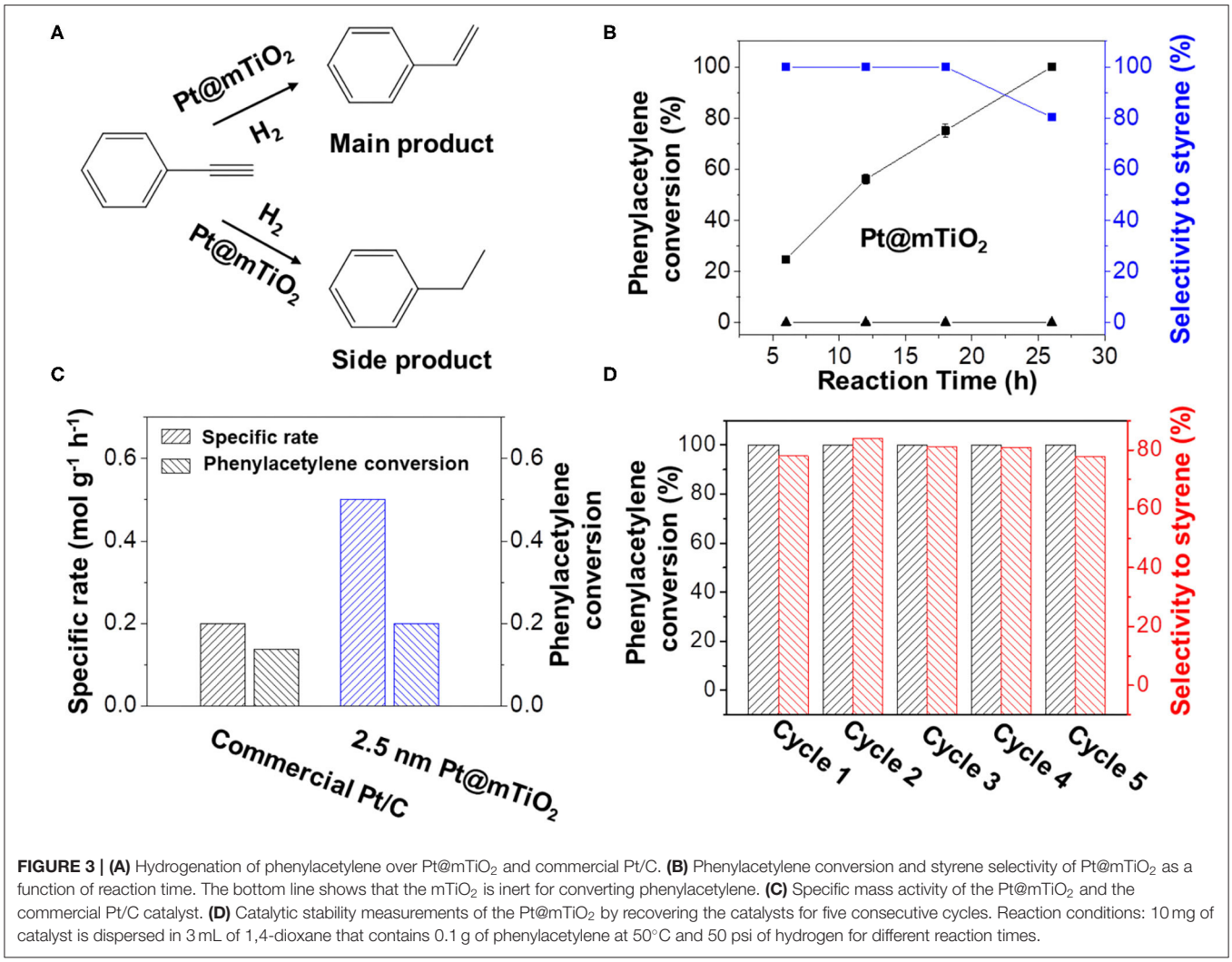

FIGURE 3 | (A) Hydrogenation of phenylacetylene over Pt@mTiO$_2$ and commercial Pt/C. **(B)** Phenylacetylene conversion and styrene selectivity of Pt@mTiO$_2$ as a function of reaction time. The bottom line shows that the mTiO$_2$ is inert for converting phenylacetylene. **(C)** Specific mass activity of the Pt@mTiO$_2$ and the commercial Pt/C catalyst. **(D)** Catalytic stability measurements of the Pt@mTiO$_2$ by recovering the catalysts for five consecutive cycles. Reaction conditions: 10 mg of catalyst is dispersed in 3 mL of 1,4-dioxane that contains 0.1 g of phenylacetylene at 50°C and 50 psi of hydrogen for different reaction times.

at around 73.1 and 77.1 eV, respectively, which may derive from surface oxidation (Miller et al., 2014). The Pt^{2+}/Pt^0 ratio, as measured from the integration areas in the fitting cure, is 0.43 for 2.5 nm Pt NPs. By comparison, this is much lower for commercial Pt/C with a Pt^{2+}/Pt^0 ratio of 0.35. This result implies that Pt is more surface oxidized in 2.5 nm Pt NPs, which is further evidenced in Ti 2p XPS spectra. As shown in **Figure 4B**, a strong Ti^{3+} XPS binding energy peak at around 458.2 eV is found in 2.5 nm Pt NPs on mTiO$_2$, which is absent in the pure mTiO$_2$ (Yang et al., 2017; Ou et al., 2018). These results show that 2.5 nm Pt NPs have a stronger interaction with the mTiO$_2$ support where Pt NPs are partially oxidized and demonstrate electron back-donation to reduce Ti^{4+} to Ti^{3+} of mTiO$_2$. The stronger metal-support interaction is of great importance in stabilizing small NPs as revealed by a series of reports (Lu and Schüth, 2006). In the current case, the excellent thermal stability of 2.5 nm Pt NPs supported on mTiO$_2$ may also derive from strong metal-support interactions.

Small NPs afford abundant surface low-coordinated corner or edge sites, which potentially modifies reactant/product adsorption modes that are quite different from that on larger ones (Zelcer and Soler-Illia, 2013). For example, alkenes prefer a weak π adsorption on low-coordinated Pt sites such as corner, edge, or single atom sites of small Pt NPs rather than a strong σ adsorption on continuous Pt lattices of larger Pt NPs. The weakening of alkene adsorption strength greatly favors high alkene selectivity (Yang et al., 2013; Zhang et al., 2019). To this end, CO-DRIFTS was further carried out to understand the high selectivity to styrene on Pt@mTiO$_2$. For the commercial Pt/C, it is very difficult to collect CO-DRIFT spectra because of signal blocking of carbon supports. Thus, we further prepared 3.6 nm Pt supported on mTiO$_2$ by calcination at a higher annealing temperature (650°C), which preserved the mesoporous structure but with slightly larger Pt NPs (3.6 nm) (**Supplementary Figure 8**). **Supplementary Figure 9** shows that both the catalytic activity and styrene selectivity of the 3.6 nm Pt NPs on mTiO$_2$ are much lower than that of the 2.5 nm Pt NPs on mTiO$_2$. **Figure 5** shows the CO-DRIFTS curve of 2.5 nm Pt NPs and 3.6 nm Pt NPs on mTiO$_2$, respectively. The CO adsorption models on 2.5 nm Pt NPs are quite different from

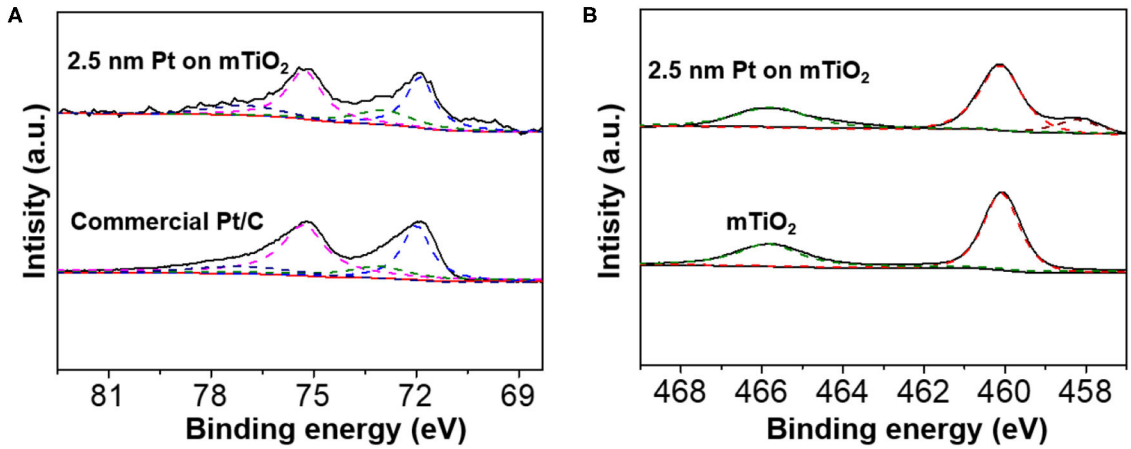

FIGURE 4 | (A) High-resolution Pt 4f XPS spectra of the 2.5 nm Pt NPs on mTiO$_2$ and commercial Pt/C. **(B)** High-resolution Ti 2p XPS spectra of the 2.5 nm Pt NPs on mTiO$_2$, and pure mTiO$_2$.

that on 3.6 nm Pt NPs. The fitted results show that only the linear CO adsorption mode is observed on the 2.5 nm Pt NPs on mTiO$_2$ while the 3.6 nm Pt NPs on mTiO$_2$ display both linear CO adsorption and bridged CO adsorption modes in the wavenumber window between 1,800 and 2,200 cm^{-1} (Singh et al., 2018). The linear CO adsorption of both 2.5 nm Pt NPs on mTiO$_2$ and 3.6 nm Pt NPs on mTiO$_2$ are related to the surface atop Pt sites (Wieckowski, 1999). Due to the Pt coordination differences, the linear CO adsorption bands of the 2.5 nm Pt NPs on mTiO$_2$ and the 3.6 nm Pt NPs on mTiO$_2$ are divided into two regions that are referred to as the low-coordination Pt-CO linear adsorption band and high-coordination Pt-CO linear adsorption band centered at around 2,004 and 2,160 cm^{-1}, respectively (Redina et al., 2015; Singh et al., 2018). The low-coordination Pt-CO linear adsorption to high-coordination Pt-CO linear adsorption ratio of 2.5 nm Pt NPs on mTiO$_2$ is calculated to be 4.8, which is 6 times higher than that of 3.6 nm Pt NPs on mTiO$_2$. This result demonstrates high unsaturated coordination of the Pt sites in 2.5 nm Pt NPs on mTiO$_2$ due to the smaller Pt NPs size as compared with 3.6 nm Pt NPs on mTiO$_2$, which agrees well with the above HAADF-STEM observations. The schematic models of Pt NPs with diameters of 2.5 and 3.6 nm are also constructed, respectively, as displayed in **Supplementary Figure 10**. Smaller Pt NPs show more abundant surface corner and edge sites, which accounts for the pure linear CO adsorption revealed via CO-DRIFTS measurements. The unique surface structures of the 2.5 nm Pt NPs on mTiO$_2$ greatly benefit weak styrene adsorption in selective hydrogenation of phenylacetylene through a π adsorption mode, which favors styrene desorption and high styrene selectivity.

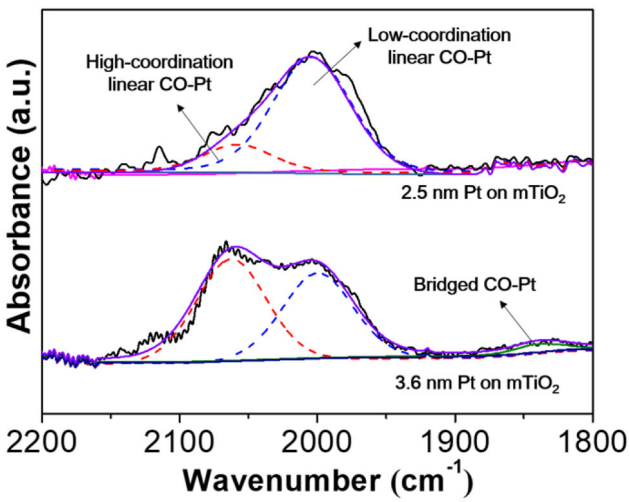

FIGURE 5 | Diffuse reflectance infrared Fourier transform spectroscopy with CO molecules of the 2.5 nm Pt NPs on mTiO$_2$ and the 3.6 nm Pt NPs on mTiO$_2$.

CONCLUSION

To summarize, we report the preparation of mesoporous TiO$_2$ confined ultrasmall Pt nanoparticles with an average particle size of 2.5 ± 0.5 nm using an EISA method. As-resulted Pt@mTiO$_2$ displayed excellent catalytic activity and styrene selectivity in semi-hydrogenation of phenylacetylene. The hydrogenation activity of Pt@mTiO$_2$ displays a 2.5-fold increase over that of the commercial Pt/C. A 100% styrene selectivity is also obtained over the Pt@mTiO$_2$ in a wide phenylacetylene conversion range of 20–75%. The styrene selectivity is remarkably above 80% even at full phenylacetylene conversion. The excellent styrene selectivity is ascribed to the abundant surface atop Pt sites as given by the CO-DRIFTS. In addition, the Pt@mTiO$_2$ also shows excellent catalytic stability as demonstrated in five consecutive recycling experiments, which shows great potential for practical

applications. Our work is expected to open up new opportunities for developing highly efficient alkene-to-alkene conversion catalysts by novel synthesis.

DATA AVAILABILITY STATEMENT

The original contributions presented in the study are included in the article/**Supplementary Material**, further inquiries can be directed to the corresponding author.

AUTHOR CONTRIBUTIONS

MH, SS, JH, and BL conceived the projects. MH carried out the experiments and analyzed data in the assist of LJ. YD did high-resolution TEM and analyzed the data. All authors co-wrote the manuscript.

ACKNOWLEDGMENTS

JH is grateful for the financial support from the University of Connecticut. The SEM/TEM studies were performed using the facilities in the UConn/Thermo Fisher Scientific Center for Advanced Microscopy and Materials Analysis (CAMMA). SS thanks the US Department of Energy, Office of Basic Energy Sciences, Division of Chemical, Biological and Geological Sciences under grant DE-FG02-86ER13622 for support of this research.

SUPPLEMENTARY MATERIAL

The Supplementary Material for this article can be found online at: https://www.frontiersin.org/articles/10.3389/fchem.2020.581512/full#supplementary-material

REFERENCES

Alig, L., Fritz, M., and Schneider, S. (2019). First-row transition metal (De)hydrogenation catalysis based on functional pincer ligands. *Chem. Rev.* 119, 2681–2751. doi: 10.1021/acs.chemrev.8b00555

Armbrüster, M., Kovnir, K., Behrens, M., Teschner, D., Grin, Y., and Schlögl, R. (2010). Pd–Ga intermetallic compounds as highly selective semihydrogenation catalysts. *J. Am. Chem. Soc.* 132, 14745–14747. doi: 10.1021/ja106568t

Behrens, M., Studt, F., Kasatkin, I., Kühl, S., Hävecker, M., Abild-Pedersen, F., et al. (2012). The active site of methanol synthesis over Cu/ZnO/Al_2O_3 industrial catalysts. *Science* 336, 893–897. doi: 10.1126/science.1219831

Borodziński, A., and Bond, G. C. (2006). Selective hydrogenation of ethyne in ethene-rich streams on palladium catalysts. Part 1. effect of changes to the catalyst during reaction. *Catal. Rev.* 48, 91–144. doi: 10.1080/01614940500364909

Borodziński, A., and Bond, G. C. (2008). Selective hydrogenation of ethyne in ethene-rich streams on palladium catalysts, Part 2: steady-state kinetics and effects of palladium particle size, carbon monoxide, and promoters. *Catal. Rev.* 50, 379–469. doi: 10.1080/01614940802142102

Cui, Y., Lian, X., Xu, L., Chen, M., Yang, B., Wu, C.-e., et al. (2019). Designing and fabricating ordered mesoporous metal oxides for CO_2 catalytic conversion: a review and prospect. *Materials* 12:276. doi: 10.3390/ma12020276

Dominguez-Dominguez, S., Berenguer-Murcia, A., Pradhan, B. K., Linares-Solano, A., and Cazorla-Amoros, D. (2008). Semihydrogenation of phenylacetylene catalyzed by palladium nanoparticles supported on carbon materials. *J. Phys. Chem. C* 112, 3827–3834. doi: 10.1021/jp710693u

Feng, Q., Zhao, S., Wang, Y., Dong, J., Chen, W., He, D., et al. (2017). Isolated single-atom pd sites in intermetallic nanostructures: high catalytic selectivity for semihydrogenation of alkynes. *J. Am. Chem. Soc.* 139, 7294–7301. doi: 10.1021/jacs.7b01471

Han, A., Zhang, J., Sun, W., Chen, W., Zhang, S., Han, Y., et al. (2019). Isolating contiguous Pt atoms and forming Pt-Zn intermetallic nanoparticles to regulate selectivity in 4-nitrophenylacetylene hydrogenation. *Nat. Commun.* 10:3787. doi: 10.1038/s41467-019-11794-6

Hu, M., Jin, L., Su, X., Bamonte, S., Lu, X., Gao, P., et al. (2020). Polymer-assisted co-assembly towards synthesis of mesoporous titania encapsulated monodisperse PdAu for highly selective hydrogenation of phenylacetylene. *ChemCatChem* 12, 1476–1482. doi: 10.1002/cctc.201901957

Hu, M., Zhang, J., Zhu, W., Chen, Z., Gao, X., Du, X., et al. (2018a). 50 ppm of Pd dispersed on Ni(OH)2 nanosheets catalyzing semi-hydrogenation of acetylene with high activity and selectivity. *Nano Res.* 11, 905–912. doi: 10.1007/s12274-017-1701-5

Hu, M., Zhao, S., Liu, S., Chen, C., Chen, W., Zhu, W., et al. (2018b). MOF-confined Sub-2 nm atomically ordered intermetallic PdZn nanoparticles as high-performance catalysts for selective hydrogenation of acetylene. *Adv. Mater.* 30:1801878. doi: 10.1002/adma.201801878

Huang, W., McCormick, J. R., Lobo, R. F., and Chen, J. G. (2007). Selective hydrogenation of acetylene in the presence of ethylene on zeolite-supported bimetallic catalysts. *J. Catal.* 246, 40–51. doi: 10.1016/j.jcat.2006.11.013

Kleis, J., Greeley, J., Romero, N., Morozov, V., Falsig, H., Larsen, A. H., et al. (2011). Finite size effects in chemical bonding: from small clusters to solids. *Catal. Lett.* 141, 1067–1071. doi: 10.1007/s10562-011-0632-0

Li, C., Shao, Z., Pang, M., Williams, C. T., and Liang, C. (2012). Carbon nanotubes supported Pt catalysts for phenylacetylene hydrogenation: effects of oxygen containing surface groups on Pt dispersion and catalytic performance. *Catal. Today.* 186, 69–75. doi: 10.1016/j.cattod.2011.09.005

Li, K., Zhao, Y., Song, C., and Guo, X. (2017). Magnetic ordered mesoporous Fe_3O_4/CeO_2 composites with synergy of adsorption and fenton catalysis. *Appl. Surf. Sci.* 425, 526–534. doi: 10.1016/j.apsusc.2017.07.041

Liu, H., Du, X., Xing, X., Wang, G., and Qiao, S. Z. (2012). Highly ordered mesoporous Cr_2O_3 materials with enhanced performance for gas sensors and lithium ion batteries. *Chem. Commun.* 48, 865–867. doi: 10.1039/C1CC16341H

Liu, X., Mou, C.-Y., Lee, S., Li, Y., Secrest, J., and Jang, B. W.-L. (2012). Room temperature O_2 plasma treatment of SiO_2 supported Au catalysts for selective hydrogenation of acetylene in the presence of large excess of ethylene. *J. Catal.* 285, 152–159. doi: 10.1016/j.jcat.2011.09.025

Lu, A.-H., and Schüth, F. (2006). Nanocasting: a versatile strategy for creating nanostructured porous materials. *Adv. Mater.* 18, 1793–1805. doi: 10.1002/adma.200600148

Mastalir, A., Király, Z., Szöllosi, G., and Bartok, M. (2000). Preparation of organophilic Pd–montmorillonite, an efficient catalyst in alkyne semihydrogenation. *J. Catal.* 194, 146–152. doi: 10.1006/jcat.2000.2929

McCue, A. J., and Anderson, J. A. (2015). Recent advances in selective acetylene hydrogenation using palladium containing catalysts. *Front. Chem. Sci. Eng.* 9, 142–153. doi: 10.1007/s11705-015-1516-4

Miller, D., Sanchez Casalongue, H., Bluhm, H., Ogasawara, H., Nilsson, A., and Kaya, S. (2014). Different reactivity of the various platinum oxides and chemisorbed oxygen in CO oxidation on Pt(111). *J. Am. Chem. Soc.* 136, 6340–6347. doi: 10.1021/ja413125q

Mitsudome, T., Urayama, T., Yamazaki, K., Maehara, Y., Yamasaki, J., Gohara, K., et al. (2016). Design of core-Pd/shell-Ag nanocomposite catalyst for selective semihydrogenation of alkynes. *ACS Catal.* 6, 666–670. doi: 10.1021/acscatal.5b02518

Montesano Lopez, R. (2014). *Selectivity and Deactivation in the Single-stage Synthesis of Dimethyl Ether from $CO_2/CO/H_2$*. Imperial College London. doi: 10.25560/26597

Ou, G., Xu, Y., Wen, B., Lin, R., Ge, B., Tang, Y., et al. (2018). Tuning defects in oxides at room temperature by lithium reduction. *Nat. Commun.* 9:1302. doi: 10.1038/s41467-018-03765-0

Pei, G. X., Liu, X. Y., Yang, X., Zhang, L., Wang, A., Li, L., et al. (2017). Performance of Cu-alloyed pd single-atom catalyst for semihydrogenation of acetylene under simulated front-end conditions. *ACS Catal.* 7, 1491–1500. doi: 10.1021/acscatal.6b03293

Prinz, J., Pignedoli, C. A., Stöckl, Q. S., ArmbrÃster, M., Brune, H., Gröning, O., et al. (2014). Adsorption of small hydrocarbons on the three-fold PdGa surfaces: the road to selective hydrogenation. *J. Am. Chem. Soc.* 136, 11792–11798. doi: 10.1021/ja505936b

Qiao, B., Wang, A., Yang, X., Allard, L. F., and Zhang, T. (2011). Single-atom catalysis of CO oxidation using Pt_1/FeO_x. *Nat. Chem.* 3, 634–641. doi: 10.1038/nchem.1095

Redina, E., Greish, A., Novikov, R., Strelkova, A., Kirichenko, O., Tkachenko, O., et al. (2015). Au/Pt/TiO_2 catalysts prepared by redox method for the chemoselective 1,2-propanediol oxidation to lactic acid and an NMR spectroscopy approach for analyzing the product mixture. *Appl. Catal. A* 491, 170–183. doi: 10.1016/j.apcata.2014.11.039

Sheng, B., Hu, L., Yu, T., Cao, X., and Gu, H. (2012). Highly-dispersed ultrafine Pt nanoparticles on graphene as effective hydrogenation catalysts. *RSC Adv.* 2, 5520–5523. doi: 10.1039/c2ra20400b

Singh, J. A., Yang, N., Liu, X., Tsai, C., Stone, K. H., Johnson, B., et al. (2018). Understanding the active sites of CO hydrogenation on Pt–Co catalysts prepared using atomic layer deposition. *J. Phys. Chem. C* 122, 2184–2194. doi: 10.1021/acs.jpcc.7b10541

Studt, F., Abild-Pedersen, F., Bligaard, T., Sørensen, R. Z., Christensen, C. H., and Nørskov, J. K. (2008). Identification of non-precious metal alloy catalysts for selective hydrogenation of acetylene. *Science* 320, 1320–1322. doi: 10.1126/science.1156660

Tang, Q., Angelomé, P. C., Soler-Illia, G. J., and Müller, M. (2017). Formation of ordered mesostructured TiO_2 thin films: a soft coarse-grained simulation study. *Phys. Chem. Chem. Phys.* 19, 28249–28262. doi: 10.1039/C7CP05304E

Tauster, S. J., Fung, S. C., and Garten, R. L. (1978). Strong metal-support interactions. Group 8 noble metals supported on titanium dioxide. *J. Am. Chem. Soc.* 100, 170–175. doi: 10.1021/ja00469a029

Teschner, D., Borsodi, J., Wootsch, A., Révay, Z., Hävecker, M., Knop-Gericke, A., et al. (2008). The roles of subsurface carbon and hydrogen in palladium-catalyzed alkyne hydrogenation. *Science* 320, 86–89. doi: 10.1126/science.1155200

Tüysüz, H., Hwang, Y. J., Khan, S. B., Asiri, A. M., and Yang, P. (2013). Mesoporous CO_3O_4 as an electrocatalyst for water oxidation. *Nano Res.* 6, 47–54. doi: 10.1007/s12274-012-0280-8

Wan, Y., and Zhao, D. (2007). On the controllable soft-templating approach to mesoporous silicates. *Chem. Rev.* 107, 2821–2860. doi: 10.1021/cr068020s

Wang, H., Guo, W., Jiang, Z., Yang, R., Jiang, Z., Pan, Y., et al. (2018). New insight into the enhanced activity of ordered mesoporous nickel oxide in formaldehyde catalytic oxidation reactions. *J. Catal.* 361, 370–383. doi: 10.1016/j.jcat.2018.02.023

Wang, J., Tan, H., Yu, S., and Zhou, K. (2015). Morphological effects of gold clusters on the reactivity of ceria surface oxygen. *ACS Catal.* 5, 2873–2881. doi: 10.1021/cs502055r

Wei, X., Shao, B., Zhou, Y., Li, Y., Jin, C., Liu, J., et al. (2018). Geometrical structure of the gold–iron(III) oxide interfacial perimeter for CO oxidation. *Angew. Chem. Int. Edit.* 57, 11289–11293. doi: 10.1002/anie.201805975

Wieckowski, A. (1999). *Interfacial Electrochemistry: Theory: Experiment, and Applications*. New York, NY: CRC Press.

Wu, S. M., Yang, X. Y., and Janiak, C. (2019). Confinement effects in zeolite-confined noble metals. *Angew. Chem. Int. Edit.* 131, 12468–12482. doi: 10.1002/ange.201900013

Xiang, S.-C., Zhang, Z., Zhao, C.-G., Hong, K., Zhao, X., Ding, D.-R., et al. (2011). Rationally tuned micropores within enantiopure metal-organic frameworks for highly selective separation of acetylene and ethylene. *Nat. Commun.* 2:204. doi: 10.1038/ncomms1206

Xiao, Y., Zheng, X., Chen, X., Jiang, L., and Zheng, Y. (2017). Synthesis of Mg-doped ordered mesoporous Pd–Al_2O_3 with different basicity for CO, NO, and HC elimination. *Ind. Eng. Chem. Res.* 56, 1687–1695. doi: 10.1021/acs.iecr.6b03799

Xie, Y., Kocaefe, D., Chen, C., and Kocaefe, Y. (2016). Review of research on template methods in preparation of nanomaterials. *J. Nanomater.* 2016:2302595. doi: 10.1155/2016/2302595

Yang, B., Burch, R., Hardacre, C., Headdock, G., and Hu, P. (2012). Origin of the increase of activity and selectivity of nickel doped by Au, Ag, and Cu for acetylene hydrogenation. *ACS Catal.* 2, 1027–1032. doi: 10.1021/cs2006789

Yang, J., Zhu, Y., Fan, M., Sun, X., Wang, W. D., and Dong, Z. (2019). Ultrafine palladium nanoparticles confined in core–shell magnetic porous organic polymer nanospheres as highly efficient hydrogenation catalyst. *J. Colloid Interface Sci.* 554, 157–165. doi: 10.1016/j.jcis.2019.07.006

Yang, P., Zhao, D., Margolese, D. I., Chmelka, B. F., and Stucky, G. D. (1998). Generalized syntheses of large-pore mesoporous metal oxides with semicrystalline frameworks. *Nature* 396, 152–155. doi: 10.1038/24132

Yang, X.-F., Wang, A., Qiao, B., Li, J., Liu, J., and Zhang, T. (2013). Single-atom catalysts: a new frontier in heterogeneous catalysis. *Acc. Chem. Res.* 46, 1740–1748. doi: 10.1021/ar300361m

Yang, Y., Gao, P., Ren, X., Sha, L., Yang, P., Zhang, J., et al. (2017). Massive Ti^{3+} self-doped by the injected electrons from external Pt and the efficient photocatalytic hydrogen production under visible-light. *Appl. Catal. B Environ.* 218, 751–757. doi: 10.1016/j.apcatb.2017.07.014

Yuan, Q., Li, L.-L., Lu, S.-L., Duan, H.-H., Li, Z.-X., Zhu, Y.-X., et al. (2009). Facile synthesis of Zr-based functional materials with highly ordered mesoporous structures. *J. Phys. Chem. C* 113, 4117–4124. doi: 10.1021/jp806467c

Zelcer, A., and Soler-Illia, G. J. A. A. (2013). One-step preparation of UV transparent highly ordered mesoporous zirconia thin films. *J. Mater. Chem. C* 1, 1359–1367. doi: 10.1039/C2TC00319H

Zhan, S., Zhang, H., Zhang, Y., Shi, Q., Li, Y., and Li, X. (2017). Efficient NH_3-SCR removal of NO_x with highly ordered mesoporous WO_3-CeO_2 at low temperatures. *Appl. Catal. B-Environ.* 203, 199–209. doi: 10.1016/j.apcatb.2016.10.010

Zhang, G., Yang, D., and Sacher, E. (2007). X-ray photoelectron spectroscopic analysis of Pt nanoparticles on highly oriented pyrolytic graphite, using symmetric component line shapes. *J. Phys. Chem. C* 111, 565–570. doi: 10.1021/jp065606+

Zhang, J., Li, Y., Zhang, Y., Chen, M., Wang, L., Zhang, C., et al. (2015). Effect of support on the activity of ag-based catalysts for formaldehyde oxidation. *Sci. Rep.* 5:12950. doi: 10.1038/srep12950

Zhang, L., Jin, L., Liu, B., and He, J. (2019). Templated growth of crystalline mesoporous materials: from soft/hard templates to colloidal templates. *Front. Chem.* 7:22. doi: 10.3389/fchem.2019.00022

Zhao, D., Feng, J., Huo, Q., Melosh, N., Fredrickson, G. H., Chmelka, B. F., et al. (1998). Triblock copolymer syntheses of mesoporous silica with periodic 50 to 300 angstrom pores. *Science* 279, 548–552. doi: 10.1126/science.279.5350.548

Zhao, Y., Dong, F., Han, W., Zhao, H., and Tang, Z. (2019). The synergistic catalytic effect between graphene oxide and three-dimensional ordered mesoporous CO_3O_4 nanoparticles for low-temperature CO oxidation. *Microporous Mesoporous Mat.* 273, 1–9. doi: 10.1016/j.micromeso.2018.06.042

Zhao, Y., Tian, H., He, J., and Yang, Q. (2015). Catalytic oxidation of formaldehyde over mesoporous MnO_x-CeO_2 catalysts. *Int. J. Nanosci.* 14:1460028. doi: 10.1142/S0219581X1460028X

Conflict of Interest: The authors declare that the research was conducted in the absence of any commercial or financial relationships that could be construed as a potential conflict of interest.

Copyright © 2020 Hu, Jin, Dang, Suib, He and Liu. This is an open-access article distributed under the terms of the Creative Commons Attribution License (CC BY). The use, distribution or reproduction in other forums is permitted, provided the original author(s) and the copyright owner(s) are credited and that the original publication in this journal is cited, in accordance with accepted academic practice. No use, distribution or reproduction is permitted which does not comply with these terms.